Biochemistry

Hole Hopping through Tryptophan in Cytochrome P450

Maraia E. Ener,[†] Harry B. Gray,* and Jay R. Winkler*

Beckman Institute, California Institute of Technology, Pasadena, California 91125, United States

S *Supporting Information*

ABSTRACT: Electron-transfer kinetics have been measured in four conjugates of cytochrome P450 with surface-bound Ru-photosensitizers. The conjugates are constructed with enzymes from *Bacillus megaterium* (CYP102A1) and *Sulfolobus acidocaldarius* (CYP119). A W96 residue lies in the path between Ru and the heme in CYP102A1, whereas H76 is present at the analogous location in CYP119. Two additional conjugates have been prepared with (CYP102A1)W96H and (CYP119)H76W mutant enzymes. Heme oxidation by photochemically generated Ru^{3+} leads to P450 compound II formation when a tryptophan residue is in the path between Ru and the heme; no heme oxidation is observed when histidine occupies this position. The data indicate that heme oxidation proceeds via two-step tunneling through a tryptophan radical intermediate. In contrast, heme reduction by photochemically generated Ru^+ proceeds in a single electron tunneling step with closely similar rate constants for all four conjugates.
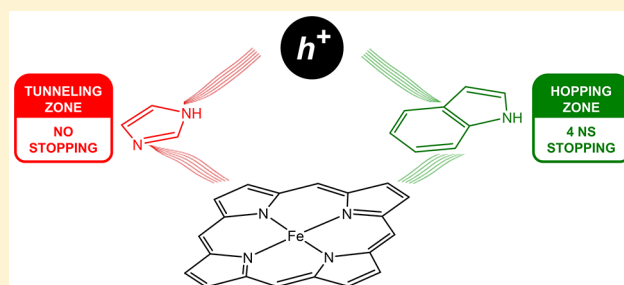
Most biological redox transformations involve reagents with formal potentials in the ±1 V vs NHE range. At the periphery of this potential window proteins present a decidedly unsymmetrical medium for electron transfer (ET). Whereas reduction of peptides and small aromatic groups only proceeds at potentials more negative than −2.5 V vs NHE,[1−3] one-electron oxidations of aromatic and sulfur-containing amino-acids, as well as the peptide backbone itself, can occur at potentials in the 1.0−1.5 V vs NHE range.[4−11] We anticipate, then, that proteins are superexchange mediators of ET in reactions of low-potential redox couples. In contrast, oxidized amino acid radicals are known to be essential participants in many high-potential enzymatic redox reactions,[12−21] and structural evidence suggests that they may play a far greater role than previously recognized.[22]

Elucidating the roles of protein radicals, particularly those of the aromatic amino acids tryptophan (W) and tyrosine (Y), in functional and protective pathways of high-potential enzymes continues to be an active area of research.[22−25] The appearance of dioxygen in Earth's atmosphere promoted the evolution of a vast array of O_2-utilizing enzymes that generate high-potential reactive intermediates capable of oxidizing tryptophan and tyrosine. The cytochromes P450 (CYP) are prominent representatives of this enzyme class, responsible for a broad spectrum of vital metabolic functions.[26] The accepted enzymatic reaction cycle of cytochrome P450 involves two high-potential reactive intermediates (compounds I and II) that participate directly in reactions with substrates.[27−32] In prior work, we demonstrated that compound II can be prepared in the heme domain of *Bacillus megaterium* P450 (CYP102A1) by oxidation of the Fe^{3+}-heme with a surface-attached Ru-(diimine)$_3^{3+}$ complex ($E°(Ru^{3+/2+}) \approx 1.2$ V vs NHE[33,34]).[35] We have extended this work to the archaeal *Sulfolobus*

acidocaldarius P450 (CYP119).[30] A key structural difference between the two enzymes is an aromatic side chain hydrogen bonded to one of the heme proprionates (W96 in CYP102A1; H76 in CYP119) (Figure 1).[36,37] We find that an intervening
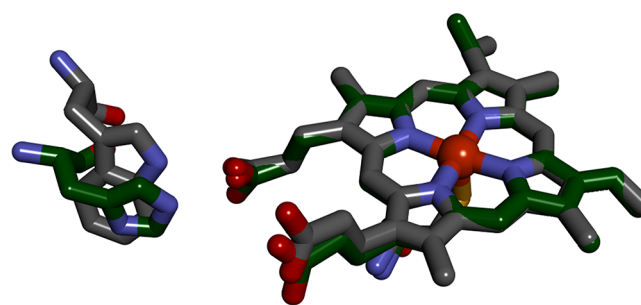
Figure 1. Overlay of the heme environments of CYP102A1 (gray carbon atoms) and CYP119 (green carbon atoms) illustrating the relative positions of W96 in CYP102A1 and H76 in CYP119. Atomic coordinates were taken from PDB IDs 2IJ2 (CYP102A1)[34] and 1IO7 (CYP119).[35]

tryptophan residue (CYP102A1, W96; CYP119, H76W) is essential for promoting $Fe^{3+}(OH_2)$−heme oxidation by Ru-(diimine)$_3^{3+}$ in both CYP102A1 and CYP119 but that these residues appear to play no analogous role in the reduction of $Fe^{3+}(OH_2)$-heme by Ru(diimine)$_3^+$ ($E°(Ru^{2+/+}) \approx −1.3$ V vs NHE[33,34]).

■ EXPERIMENTAL PROCEDURES

Materials. Buffer salts were obtained from J.T. Baker. 5-Aminolevulenic acid and dithiothreitol were obtained from Sigma-Aldrich. $[Ru(NH_3)_6]Cl_3$ was obtained from Strem Chemicals. All chemicals were used as received with no further purification. The ruthenium labeling reagent ($[Ru(2,2'-bipyridine)_2(5-iodoacetamido\ 1,10-phenanthroline)]^{2+}$, $[Ru(bpy)_2(IAphen)]^{2+}$),[38] model complex ($[Ru(2,2'-bipyridine)_2(5-acetamido\ 1,10-phenanthroline)]^{2+}$, $[Ru(bpy)_2(Aphen)]^{2+}$),[38] and p-methoxydimethylaniline (pMeODMA)[39] were synthesized according to published procedures. Solutions were prepared using 18 MΩ-cm water unless otherwise noted. Mutagenesis primers were obtained from Operon.

Plasmid Preparation. The recombinant CYP102A1 (UniProt accession number P14779) heme domain, consisting of the first 463 residues with an N-terminal 6-histidine tag, was obtained courtesy of Professor Andrew Udit (Occidental College, Los Angeles California), within the pCWori⁺ vector. Recombinant CYP119 (UniProt accession number Q55080) with an N-terminal 6-histidine tag was obtained courtesy of Professor Paul Ortiz de Montellano (University of California, San Francisco), also within the pCWori⁺ vector. Qiagen Quik-Change site-directed mutagenesis was used to generate the desired P450 mutants. Mutagenesis primers (forward, 5′−3′) were CTAATTAAGAAGCAGCCGATGAATCACG (CYP102A1 C62A), CGATTGGTCTTAGCGGCTTTAAC (CYP102A1 C156S), GCTGGACGCATCAAAAAAATTGGTGCAAAGCGC (CYP102A1 K97C); GGACGCATGAAAAAAATCATTGCAAAGCGCATAATATC (CYP102A1 W96H); GATCCCCCTCTCCATTGTGAGTTAAGATCAATGTCAGC (CYP119 D77C), and CCTCAGATCCCCCTCTCTGGTGTGAGTTAAGATCAATGTC (CYP119 H76W).

Overexpression in *E. coli*. The P450 mutants CYP102A1-C62A/C156S/K97C ($_{C97}$(CYP102A1)W96), CYP102A1-C62A/C156S/K97C/W96H ($_{C97}$(CYP102A1)W96H), CYP119-D77C ($_{C77}$(CYP119)H76), and CYP119-D77C/H76W ($_{C77}$(CYP119)H76W) were overexpressed in the BL21-DE3 strain of *E. coli*. Overnight cultures of Luria−Bertani broth (25 mL) containing 100 μg/mL ampicillin and a single respective *E. coli* colony were incubated at 37 °C overnight, shaking at 180−200 rpm. Induction cultures of TB (1× TB for CYP102A1, 2× TB for CYP119) containing 200 μg/mL ampicillin, 1 μM thiamine, 0.4% glycerol, and 250 μL of mineral supplements (stock solution 100 mM $FeCl_3$, 10 mM $ZnCl_2$, 8.5 mM $CoCl_2$, 8.5 mM Na_2MoO_4, 7 mM $CaCl_2$, 7.5 mM $CuCl_2$, 8 mM H_3BO_3) were inoculated with the overnight culture and incubated at 37 °C until reaching an optical density of ~1 at 600 nm. Cultures were induced by addition of 1 mM IPTG, and 0.5 mM α-aminolevulenic acid, a heme precursor, was added. The temperature was lowered to 30 °C for 24 (CYP102A1) or 48 h (CYP119). Following expression, cells were harvested by centrifugation, and cell pellets were stored at −80 °C until needed.

Cell pellets were resuspended in cold wash buffer (50 mM Tris pH 8, 300 mM sodium chloride, 20 mM imidazole). A small spatula tip of each of two protease inhibitors (benzamidine hydrochloride and Pefabloc SC) was added, and cells were lysed by two to three cycles of probe-tip sonication (0.5 s on, 0.5 s off, for 5 min), cooled by an ice−water bath. After centrifugation (15 000 rpm, 1 h, 8 °C) to

pellet cellular debris, the supernatant was loaded directly onto a Ni batch column. After thorough washing with wash buffer (1.5−2 L), protein was eluted (200 mM imidazole in wash buffer), and the colored (red/orange) fractions were collected and concentrated in 30 kDa centrifugal filters. Gel filtration chromatography was used to remove fragmented proteins, followed by buffer exchange into 20 mM Tris, pH 8, with 20 mM dithiothreitol (DTT) added to reduce intermolecular disulfide bonds. Purity was determined by UV−vis absorption (A_{420}/A_{280}), SDS-PAGE, and mass spectrometry. Protein not intended for immediate use was flash-frozen in liquid nitrogen (with 40% glycerol added to solution as cryoprotectant) and stored at −80 °C.

Conjugation to Ru-Photosensitizer. An approximately 3-fold excess of $[Ru(bpy)_2(IA-phen)]^{2+}$ was added to a ~10 μM solution of P450 mutant in 20 mM Tris buffer (pH 8) and shaken in the dark at 4 °C. Labeling progress can be monitored by MALDI mass spectrometry; no further increase in the peak corresponding to the predicted mass of Ru^{2+}−P450 was observed after 2 h. Excess $[Ru(bpy)_2(IA-phen)]^{2+}$ was removed during concentration in 30 kDa filters, followed by desalting on an FPLC HiPrep column.

To separate photosensitizer-labeled and unlabeled enzymes, protein samples were loaded onto an anion exchange MonoQ or HiPrep Q column equilibrated with 20 mM Tris buffer, pH 8 (Q wash buffer). The column was washed with Q wash buffer until UV−visible absorbance returned to baseline. The gradient was ramped quickly to 59% Q elution buffer (Q wash buffer + 250 mM sodium chloride), followed by a slow gradient of 59−65% Q elution buffer over 60 min. Successful conjugation and separation of Ru−P450 was verified by UV−vis, mass spectrometry, and fluorometry.

Laser Spectroscopy Sample Preparation. Laser samples were composed of ~10 μM Ru−P450 conjugate, with and without oxidative quencher (17 mM $[Ru(NH_3)_6]Cl_3$) or reductive quencher (10 mM pMeODMA) in buffered solution (pH 8, 50 mM sodium borate or 50 mM Tris); additionally, each buffer contained sodium chloride to prevent precipitation. pMeODMA is only sparingly soluble in water; aqueous stock solutions were prepared by dropwise addition of concentrated pMeODMA/DMSO solution into aqueous buffer (50 mM sodium borate, pH 8). Fresh pMeODMA solutions were prepared immediately prior to use and protected from light, as oxygenated solutions change from clear to pinkish/purple in ambient light. Laser samples were placed in a high-vacuum four-sided quartz fluorescence cuvette with high-vacuum Teflon valve, equipped with a small stir bar. Deoxygenation was achieved via 3 × 10−15 gentle pump-backfill cycles with argon on a Schlenk line, with 15 min of equilibration between each set of cycles. Additional details provided in Supporting Information.

For nanosecond-to-millisecond transient luminescence and absorption experiments, excitation was provided by 480 nm pulses from a tunable optical parametric oscillator (Spectra Physics, Quanta-Ray MOPO-700) pumped by the third harmonic from a Spectra Physics Q-switched Nd:YAG laser (Spectra-Physics, Quanta-Ray PRO-Series, 8 ns pulse width) operated at 10 Hz. Probe light was provided by a 75-W arc lamp (PTI model A 1010) that could be operated in continuous or pulsed mode and passed through the sample collinearly with the excitation pulse. After rejection of scattered light by appropriate long- and short-pass filters, and intensity modulation by a neutral density filter, probe wavelengths were

Table 1. Luminescence Decay Times of Four Ru−P450 Conjugates in the Absence and Presence of Quenchers[a]

enzyme	quencher	τ_{mono}, ns	τ_a, ns (ρ_a)	τ_b, ns (ρ_b)
Ru$_{C97}$(CYP102A1)W96	none	140	190 (0.65)	52 (0.35)
	[Ru(NH$_3$)$_6$]$^{3+}$	30		
	pMeODMA	62		
Ru$_{C97}$(CYP102A1)W96H	none	180	160 (0.80)	310 (0.20)
	[Ru(NH$_3$)$_6$]$^{3+}$	33		
	pMeODMA	65		
Ru$_{C77}$(CYP119)H76	none	200	220 (0.85)	45 (0.15)
	[Ru(NH$_3$)$_6$]$^{3+}$	91		
	pMeODMA	54		
Ru$_{C77}$(CYP119)H76W	none	130	91 (0.75)	320 (0.25)
	[Ru(NH$_3$)$_6$]$^{3+}$	48		
	pMeODMA	50		

[a]Quenchers: [Ru(NH$_3$)$_6$]$^{3+}$, 17 mM; pMeODMA, 10 mM. The relative amplitudes of major (ρ_a) and minor (ρ_b) components in biexponential fits to the unquenched decays also are listed. Samples were excited at 480 nm, and luminescence was detected at 630 nm. Uncertainties in the decay times are ±10%, except for the single-exponential fits to the unquenched decays.

selected by a double monochromator (Instruments SA DH-10) with 1 mm slits. Transmitted light was detected by a photomultiplier tube (PMT, Hamamatsu R928) and amplified by a 200 MHz wideband voltage amplifier DHPVA-200 (FEMTO).

Luminescence decays were monitored at 630 nm. Single wavelength transient absorption kinetics were monitored every 10 nm from 390 to 440 nm, averaging ∼500 shots per wavelength. Data from five separate time scales (2 μs, 40 μs, 400 μs, 10 ms, and 500 ms) were collected, log-compressed, and spliced together to produce full kinetics traces using Matlab software (Mathworks).

■ RESULTS

Ru−P450 Conjugates. Electron-transfer kinetics measurements were performed on four Ru−P450 conjugates: two mutants of CYP102A1 and two of CYP119. The Ru−P450 from our previous work is a triple mutant of CYP102A1: C62A/C156S/K97C with [Ru(2,2′-bipyridine)$_2$(5-acetamido-1,10-phenanthroline)]$^{2+}$ ([Ru(bpy)$_2$(APhen)]$^{2+}$) covalently bound to C97 via a thioether linkage (Ru$_{C97}$(CYP102A1)W96). To investigate the importance of W96 in photochemical ET, we generated the analogous conjugate with a W96H mutation (Ru$_{C97}$(CYP102A1)W96H). The W96H mutation should preserve hydrogen-bonding with the heme propionates, which is thought to provide structural stability to the heme.[40] But, unlike tryptophan, this side chain should not be susceptible to oxidation by photochemically generated Ru^{3+}.[11]

We have prepared analogous Ru−P450 conjugates with an intervening histidine or tryptophan residue in thermophilic CYP119. The residue corresponding to CYP102A1-W96 is H76 in CYP119 (Figure 1); a cysteine mutation at residue 77 serves as the photosensitizer attachment point. The two Ru−CYP119 conjugates are referred to as Ru$_{C77}$(CYP119)H76 and Ru$_{C77}$(CYP119)H76W.

Luminescence Quenching Measurements. The Ru(diimine)$_3$ photosensitizer luminesces upon 480 nm excitation. The luminescence decay of all four Ru−P450 conjugates is nonexponential, attributable to multiple photosensitizer conformations that do not exchange on the luminescence decay time scale. The nonexponential decay kinetics are most pronounced for mutants containing a tryptophan residue adjacent to the Ru-tethering point (Ru$_{C97}$(CYP102A1)W96, Ru$_{C77}$(CYP119)H76W). The mild oxidant [Ru(NH$_3$)$_6$]$^{3+}$ is an

efficient quencher of excited Ru(diimine)$_3$$^{2+}$ complexes (*Ru^{2+}),[35] producing powerfully oxidizing Ru(diimine)$_3$$^{3+}$ in high yield. In the presence of [Ru(NH$_3$)$_6$]$^{3+}$ (17 mM), luminescence is strongly quenched, and the decay kinetics can be fit to a single exponential function (Table 1). There are small differences in quenched decay times; in particular, the decay time of quenched Ru$_{C77}$(CYP119)H76 is approximately two to three times longer than that found in the three other proteins (90 ns vs 30−50 ns). The origin of this difference is not readily apparent.

In prior work, we demonstrated that *para*-methoxy-N,N-dimethylaniline (pMeODMA) quenches *Ru^{2+} complexes to produce one-electron reduced forms (Ru^{+}).[39] In the presence of 10 mM pMeODMA, *Ru^{2+} luminescence is efficiently quenched, and the decay kinetics are monoexponential. In contrast to the oxidative quenching with [Ru(NH$_3$)$_6$]$^{3+}$, there is very little difference in the quenched decay times among the four Ru−P450 conjugates (Table 1).

Transient Absorption Measurements. In the absence of electron-transfer quenchers, the transient absorption features of the Ru−P450 conjugates are characterized by a loss of Ru(diimine)$_3$$^{2+}$ metal-to-ligand charge transfer (MLCT) absorbance in the 400−440 nm region due to depopulation of the ground-state photosensitizer. The spectral and temporal profiles of these transients are essentially identical for the free photosensitizer and all four Ru−P450 conjugates: the features return to baseline with the same time constants as the luminescence decay.

Oxidative Quenching. Transient absorption measurements demonstrate that [Ru(NH$_3$)$_6$]$^{3+}$ quenches the *Ru^{2+} to produce electron-transfer products (Figure 2). The ligand field absorption bands of [Ru(NH$_3$)$_6$]$^{3+/2+}$ are too weak to make any detectable contribution to the transient spectra. Photogenerated [Ru(bpy)$_2$(APhen)]$^{3+}$ (Ru^{3+}) is characterized by a bleach of [Ru(bpy)$_2$(APhen)]$^{2+}$ MLCT absorption between 390 and 440 nm, and time-resolved absorption measurements reveal that it persists for several microseconds before reacting with [Ru(NH$_3$)$_6$]$^{2+}$ to regenerate the Ru^{2+} sensitizer and oxidized quencher (Figure 2).

We reported previously that when [Ru(bpy)$_2$(IAphen)]$^{2+}$ is conjugated to C97 in CYP102A1, photogenerated Ru$_{C97}$$^{3+}$(CYP102A1)W96 sequentially generates ferric-porphyrin radical cation (Fe^{3+}por$^{•+}$) and Fe^{4+}-hydroxide (Fe^{4+}−OH, CII) intermediates. These oxidation processes are characterized
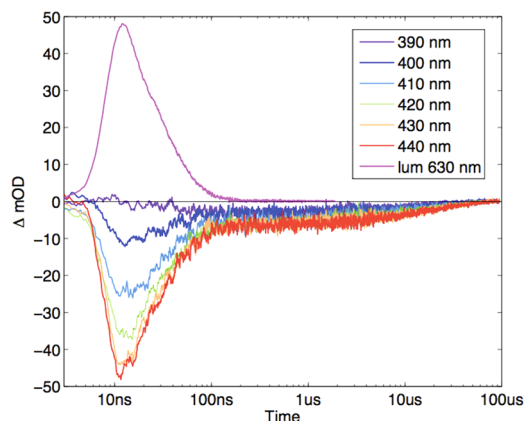
Figure 2. Transient absorption kinetics following 480 nm laser excitation of $[Ru(bpy)_2(Aphen)]^{2+}$ in the presence of $[Ru(NH_3)_6]^{3+}$ (17 mM). The purple curve is a luminescence decay trace.

by loss of absorbance at 420 nm (the peak of the $Fe^{3+}-OH_2$ heme Soret absorption) that persists for hundreds of milliseconds; formation of CII is characterized by the appearance of transient absorption at 440 nm on the millisecond time scale (Figure 3).

We subjected the other three Ru−P450 conjugates to identical oxidative flash-quench irradiation and recorded the transient kinetics (Figure 3). The CYP119 mutant with an intervening tryptophan, $Ru_{C77}(CYP119)H76W$, displays transient absorption spectra and kinetics similar to those of $Ru_{C97}(CYP102A1)W96$, albeit with smaller signal amplitudes (<5 mOD) (Figure 3). The lower ET yield in this variant may be a consequence of nonproductive oxidation of other nearby aromatic residues or less efficient competition with back electron transfer from reduced quencher. The results with $Ru_{C97}(CYP102A1)W96$ and $Ru_{C77}(CYP119)H76W$ are in striking contrast to those of the Ru−P450 constructs with an intervening histidine residue ($Ru_{C97}(CYP102A1)W96H$ and $Ru_{C77}(CYP119)H76$). Neither of the latter constructs reveals any evidence indicative of heme oxidation following photochemical generation of the $Ru(diimine)_3^{3+}$ complex. In both cases, we observe only a bleach of the ground-state MLCT absorption features (390−440 nm) that returns to baseline within 200 μs. The spectral profiles and kinetics of these transients are nearly identical to that of the free photosensitizer ($[Ru(bpy)_2(Aphen)]^{2+}$) quenched with $[Ru(NH_3)_6]^{3+}$ (Figure 2). These observations suggest that $Ru(diimine)_3^{3+}$ oxidizes the P450 heme only in structures with an intervening tryptophan residue.

Reductive Quenching. Photochemical reduction of Ru−P450 conjugates was performed using pMeODMA as quencher. The resulting Ru^+ species has nearly 1 eV of driving force for reduction of the ferric P450 heme: $E°(Ru(bpy)_3^{2+/+}) = -1.3$ V vs NHE;[33,34] $E°(P450\ Fe^{3+/2+}) = -0.43$ V vs NHE.[41] All four Ru−P450 conjugates exhibit similar transient absorption features under flash-quench conditions (Figure 4). Three distinct kinetics phases appear on the nanosecond, microsecond, and millisecond time scales following pulsed laser excitation of the photosensitizer. All transient absorption features decay back to baseline within a few hundred milliseconds, suggesting that the overall photochemical process is reversible. The fastest kinetics phase ($\tau \approx 60$ ns) is assigned to decay of $*Ru(diimine)_3^{2+}$; transient absorption features associated with this state decay with the same time constant as the luminescence. Transient absorption at 510 nm, attributable
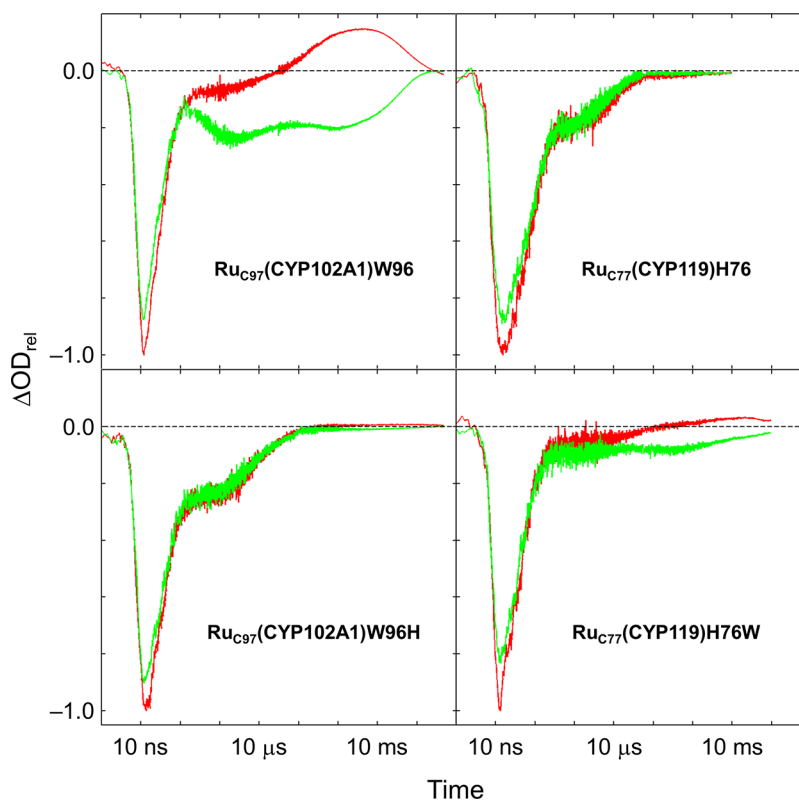
Figure 3. Transient kinetics following oxidative quenching ($[Ru(NH_3)_6]^{3+}$, 17 mM) in four Ru−P450 conjugates: $\lambda_{ex} = 480$ nm; $\lambda_{obsd} = 420$ nm (green), 440 nm (red). Signals normalized to the magnitude of the 440 nm prompt bleach.
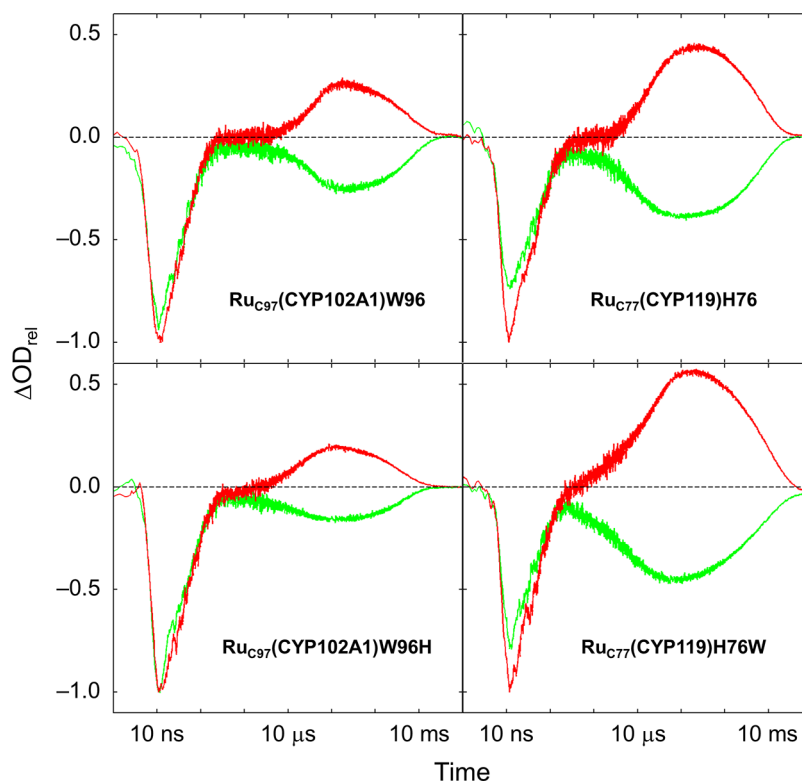
Figure 4. Transient kinetics following reductive quenching (*p*MeODMA, 10 mM) of four Ru−P450 conjugates: λ_{ex} = 480 nm; λ_{obsd} = 420 nm (green), 440 nm (red). Signals normalized to the magnitude of the 440 nm prompt bleach.

to Ru(diimine)$_3^+$ and *p*MeODMA$^{\bullet+}$, develops with the same time constant. The subsequent microsecond kinetics phase is characterized by a bleach at 420 nm and increased absorbance at 440 nm, indicative of a red-shift in the heme Soret band. In the resting state of Fe^{3+}-P450, the Fe center is axially ligated by cysteine thiolate and water ligands, producing a low-spin electronic configuration. Chemical reduction of Fe^{3+}-P450 produces a five-coordinate high-spin ferrous heme with a blue-shifted Soret band.[41] The red-shifted Soret observed following reductive quenching of the Ru−P450 conjugates is indicative of a low-spin ferrous heme.[42] The microsecond heme reduction by Ru$^+$ is likely faster than aquo ligand loss, resulting in a transient low-spin, six-coordinate ferrous species. This conclusion is consistent with the absorption profiles of Fe^{2+}(CO)−CYP101 (P450$_{cam}$ from *Pseudomonas putida*), Fe^{2+}(imidazole)−CYP101, and cryoreduced CYP101.[43,44] The millisecond kinetics phase corresponds to reoxidation of the reduced heme by *p*MeODMA$^{\bullet+}$, resulting in a return to baseline of all transient absorption features and regeneration of Fe^{3+}(OH$_2$)−P450 and *p*MeODMA.

We performed a global least-squares analysis of the Ru−P450 reductive quenching kinetics recorded at 420 and 440 nm (and, for select mutants, 400, 410, 430 nm) to a three-exponential function with amplitude coefficients $\rho_{1-3}(\lambda)$ and rate constants γ_{1-3} (eq 1). We fixed the first observed rate constant to the value obtained from single-exponential fits to the quenched luminescence decay kinetics recorded at 630 nm. The remaining two rate constants, which were extracted from the global fitting, are listed in Table 2.

$$\Delta OD(\lambda, t) = \rho_1(\lambda) \, e^{-\gamma_1 t} + \rho_2(\lambda) \, e^{-\gamma_2 t} + \rho_3(\lambda) \, e^{-\gamma_3 t} \quad (1)$$

The second rate constant corresponds to heme reduction. All four mutants exhibit very similar reduction rates, with

Table 2. Rate Constants for Ru-Sensitizer Quenching (γ_1), Heme Reduction (γ_2), and Heme Oxidation (γ_3) Extracted from Global Fitting of Transient Absorption Data

| enzyme	γ_1 (s^{-1})	γ_2 (s^{-1})	γ_3 (s^{-1})
Ru$_{C97}$(CYP102A1)W96	1.6×10^7	3.6×10^4	1.1×10^2
Ru$_{C97}$(CYP102A1)W96H	1.6×10^7	6.0×10^4	1.9×10^2
Ru$_{C77}$(CYP119)H76	1.9×10^7	5.7×10^4	1.4×10^2
Ru$_{C77}$(CYP119)H76W	1.9×10^7	8.1×10^4	1.3×10^2

maximum heme reduction complete at approximately 100 μs. Interestingly, after normalizing by the magnitude of the prompt *Ru^{2+} excited state bleach (440 nm), the magnitudes of the transient features associated with heme reduction (e.g., absorption at 440 nm) differ greatly among the four Ru−P450 conjugates. In particular, both CYP119 mutants exhibit absorption features that are greater by a factor of 2−3 than either of the CYP102A1 mutants (Figure 4).

All transient absorption features decay to baseline within 100 ms; this return rate is extremely sensitive to small amounts of oxygen. In our proposed flash-quench scheme, reoxidation of the ferrous center occurs via bimolecular recombination with *p*MeODMA$^{\bullet+}$. This recombination is expected to be a second-order process; however, the disappearance of the transient features is better modeled as a first-order process, possibly owing to reaction with oxygen or minor impurities.

■ DISCUSSION

In a prior report on the kinetics of heme oxidation by Ru^{3+} in Ru$_{C97}$(CYP102A1)W96, we found spectroscopic evidence for stepwise oxidation of Fe^{3+}(OH$_2$)−heme to Fe^{4+}(OH)−heme via an intermediate porphyrin radical cation. Electron transfer from the porphyrin to Ru$^{3+}_{C97}$ was remarkably rapid (8.5×10^5

s^{-1}, pH 8), given the 20.8-Å distance from the Ru-center to the nearest aromatic carbon atom on the porphyrin ring (Figure 5).[35] This result conflicts with the semiclassical ET theory
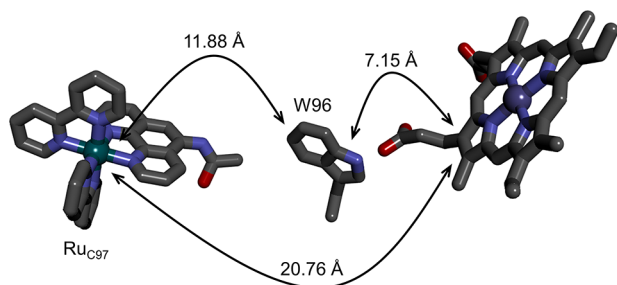
Figure 5. Structural model of Ru$_{C97}$−CYP102A1 (PDB ID 3NPL) highlighting the electron-transfer distances from Ru$_{C97}$ to the porphryin (20.76 Å), Ru$_{C97}$ to W96 (11.88 Å), and W96 to the porphyrin (7.15 Å).

prediction that the rate constant for this reaction should be 3 orders of magnitude smaller (4×10^2 s^{-1}; $-\Delta G^\circ$ = 0.2 eV; reorganization energy λ = 0.8 eV; distance decay factor β = 1.1 Å^{-1}, see Supporting Information). Indeed, the failure to observe flash-quench induced heme oxidation in Ru$_{C77}$(CYP119)H76 is in better agreement with the slower predicted rate since porphyrin oxidation by Ru^{3+} apparently does not compete effectively with Ru^{3+} reduction by reduced quencher (complete in 100 μs).

The fact that we observe flash-quench heme oxidation only in Ru−P450s with intervening tryptophan residues strongly implicates the tryptophan radical cation as a reaction intermediate. Kinetics modeling of a stepwise hole-transfer reaction from Ru^{3+} to W96$^{\bullet+}$ to por$^{\bullet+}$, using distances taken from the Ru$_{C97}$(CYP102A1)W96 structure (PDB ID 3NPL)[35] (Figure 5), predicts an apparent rate constant for porphyrin

oxidation of 1.4×10^6 s^{-1} (Supporting Information), a value in remarkably good agreement with the experimentally derived quantity. The rate constant for hole transfer from W96$^{\bullet+}$ to por$^{\bullet+}$ is predicted to be more than 2 orders of magnitude greater, suggesting that a negligibly small concentration of W96$^{\bullet+}$ will build up during the porphyrin oxidation process (Figure 6).

The kinetics of the high-potential heme oxidation reaction are in striking contrast to those of the low-potential heme reduction reaction. The estimated driving force for the Ru$^+$ to Fe^{3+}(OH$_2$)−heme ET is 0.9 eV, close to the reorganization energy estimate of 0.8 eV. The ET distance is somewhat ambiguous for this reaction because the transferring electron could be localized on any one of the three diimine ligands. On the basis of the Ru$_{C97}$(CYP102A1) crystal structure,[35] the shortest distances from any diimine ligand to the Fe center range from 19.5 to 23.8 Å. Semiclassical ET theory predicts that the rate constant for reactions over this distance range will be 10^3–10^5 s^{-1}, in accord with the γ_2 values listed in Table 2. Moreover, the rate constants for heme reduction vary by no more than a factor of 2 among the four conjugates. We conclude from this analysis that reduction of Fe^{3+}(OH$_2$)−heme by Ru$_{C97}^+$ in CYP102A1 and by Ru$_{C77}^+$ in CYP119 involves single step electron tunneling and that the intervening tryptophan (W96, W76) and histidine (H96, H76) residues serve only to mediate the superexchange coupling between the two redox sites (Figure 6).

The heme oxidation and reduction kinetics in Ru$_{C97}$(CYP102A1) and Ru$_{C77}$(CYP119) highlight the asymmetry between high and low potential ET reactions in proteins. The electron-tunneling timetables extracted from our studies of ET in Ru-modified proteins provide benchmarks for single-step electron tunneling in which the reduction potential of the oxidant is <1 V vs NHE. Our studies of Ru−P450 clearly demonstrate that multistep tunneling reactions via tryptophan
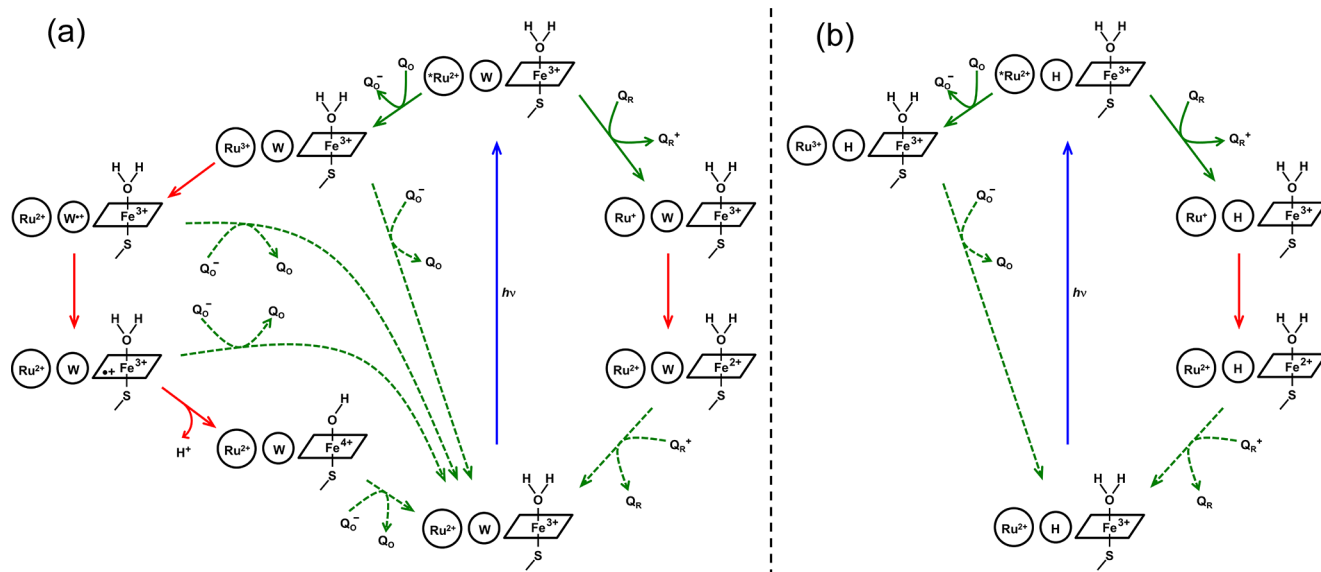
Figure 6. Photochemical ET reaction scheme in Ru$_{C97}$(CYP102A1) and Ru$_{C77}$(CYP119). Blue arrows indicate excitation processes, solid green arrows indicate bimolecular quenching reactions, dashed green arrows indicate bimolecular charge-recombination processes with quencher redox products, and red arrows indicate intraprotein ET reactions. With an intervening W residue (a, CYP102A, W96; CYP119 H76W), oxidative quenching of *Ru^{2+} by Q$_O$ (left path) leads to heme oxidation via an intermediate Trp radical; reductive quenching by Q$_R$ (right path) leads to heme reduction in a single-step tunneling reaction. With an intervening H residue (b, CYP102A, W96H; CYP119 H76), oxidative quenching of *Ru^{2+} by Q$_O$ produces Ru^{3+} but not heme oxidation, whereas reductive quenching again leads to single-step electron transfer from Ru$^+$ to the heme.

(and tyrosine) radicals come into play when oxidants have potentials >1 V. In addition, the radicals of the sulfur-containing amino acids also might be participants in reactions with particularly high potential oxidants. For enzymes functioning with intermediates at potentials greater than 1 V, protein structure and composition are critically important factors that ensure oxidizing equivalents are delivered to intended targets rather than diffusing to low potential sinks via multistep tunneling. The obvious corollary is that strategic placement of tryptophan and tyrosine residues in enzymes can direct the flow of oxidizing equivalents over long distances with little loss of potential.

■ ASSOCIATED CONTENT

Ⓢ Supporting Information

The Supporting Information is available free of charge on the ACS Publications website at DOI: 10.1021/acs.biochem.7b00432.

> Additional experimental details, spectra of ferric and ferrous wild-type P450-BM3 and the ferrous−ferric difference spectrum, details of electron transfer rate calculations, and estimated electron transfer rate constants (PDF)

■ AUTHOR INFORMATION

Corresponding Authors

*Harry B. Gray. E-mail: hbgray@caltech.edu. Phone: 626-395-6500.

*Jay R. Winkler. E-mail: winklerj@caltech.edu. Phone: 626-395-2834.

ORCID Ⓞ

Jay R. Winkler: 0000-0002-4453-9716

Present Address

†M.E.E.: Department of Chemistry, Yale University, 225 Prospect St., P.O. Box 208107, New Haven, CT 06520, U.S.A.

Funding

Notes

The authors declare no competing financial interest.

■ ABBREVIATIONS

ET, electron transfer; MLCT, metal-to-ligand charge transfer; [Ru(bpy)$_2$(IAphen)]$^{2+}$, [Ru(2,2′-bipyridine)$_2$(5-iodoacetamido 1,10-phenanthroline)]$^{2+}$; [Ru(bpy)$_2$(Aphen)]$^{2+}$, [Ru(2,2′-bipyridine)$_2$(5-acetamido-1,10-phenanthroline)]$^{2+}$; *p*MeODMA, *p*-methoxydimethylaniline

■ REFERENCES

(1) Heinze, J. (2016) Aliphatic and Aromatic Hydrocarbons - Reduction, in *Organic Electrochemistry* (Hammerich, O., and Speiser, B., Eds.), pp 861−890, Taylor and Francis Group, Boca Raton, FL.

(2) Holton, D. M., Edwards, P. P., and Salmon, G. A. (1984) Electrons, alkali metal-electron species and radical anions in substituted organic amides. *J. Phys. Chem. 88*, 3855−3859.

(3) Knecht, L. A., and Kolthoff, I. M. (1962) N-Methylacetamide as a Polarographic Solvent. *Inorg. Chem. 1*, 195−203.

(4) Harriman, A. (1987) Further Comments on the Redox Potentials of Tryptophan and Tyrosine. *J. Phys. Chem. 91*, 6102−6104.

(5) Fourré, I., Bergès, J., and Houée-Levin, C. (2010) Structural and Topological Studies of Methionine Radical Cations in Dipeptides: Electron Sharing in Two-Center Three-Electron Bonds. *J. Phys. Chem. A 114*, 7359−7368.

(6) Glass, R. S., Hug, G. L., Schoneich, C., Wilson, G. S., Kuznetsova, L., Lee, T. M., Ammam, M., Lorance, E., Nauser, T., Nichol, G. S., and Yamamoto, T. (2009) Neighboring Amide Participation in Thioether Oxidation: Relevance to Biological Oxidation. *J. Am. Chem. Soc. 131*, 13791−13805.

(7) Glass, R. S., Petsom, A., Hojjatie, M., Coleman, B. R., Duchek, J. R., Klug, J., and Wilson, G. S. (1988) Facilitation of Electrochemical Oxidation of Dialkyl Sulfides Appended with Neighboring Carboxylate and Alcohol Groups. *J. Am. Chem. Soc. 110*, 4772−4778.

(8) Jovanovic, S. V., Harriman, A., and Simic, M. G. (1986) Electron-Transfer Reactions of Tryptophan and Tyrosine Derivatives. *J. Phys. Chem. 90*, 1935−1939.

(9) Surdhar, P. S., and Armstrong, D. A. (1987) Reduction potentials and exchange reactions of thiyl radicals and disulfide anion radicals. *J. Phys. Chem. 91*, 6532−6537.

(10) Yashiro, H., White, R. C., Yurkovskaya, A. V., and Forbes, M. D. E. (2005) Methionine radical cation: Structural studies as a function of pH using X- and Q-band time-resolved electron paramagnetic resonance spectroscopy. *J. Phys. Chem. A 109*, 5855−5864.

(11) Navaratnam, S., and Parsons, B. J. (1998) Reduction Potential of Histidine Free Radicals: a Pulse Radiolysis Study. *J. Chem. Soc., Faraday Trans. 94*, 2577−2581.

(12) Stubbe, J., and van der Donk, W. A. (1998) Protein Radicals in Enzyme Catalysis. *Chem. Rev. 98*, 705−762.

(13) Aubert, C., Mathis, P., Eker, A. P. M., and Brettel, K. (1999) Intraprotein Electron Transfer between Tyrosine and Tryptophan in DNA photolyase from *Anacystis nidulans*. *Proc. Natl. Acad. Sci. U. S. A. 96*, 5423−5427.

(14) Aubert, C., Vos, M. H., Mathis, P., Eker, A. P. M., and Brettel, K. (2000) Intraprotein Radical Transfer during Photoactivation of DNA Photolyase. *Nature 405*, 586−590.

(15) DeGray, J. A., Lassmann, G., Curtis, J. F., Kennedy, T. A., Marnett, L. J., Eling, T. E., and Mason, R. P. (1992) Spectral-Analysis of the Protein-Derived Tyrosyl Radicals from Prostaglandin-H Synthase. *J. Biol. Chem. 267*, 23583−23588.

(16) Eklund, H., Eriksson, M., Uhlin, U., Nordlund, P., and Logan, D. (1997) Ribonucleotide Reductase - Structural Studies of a Radical Enzyme. *Biol. Chem. 378*, 821−825.

(17) Goodin, D. B., Mauk, A. G., and Smith, M. (1986) Studies of the Radical Species in Compound ES of Cytochrome c Peroxidase Altered by Site-Directed Mutagenesis. *Proc. Natl. Acad. Sci. U. S. A. 83*, 1295−1299.

(18) Green, M. T. (1999) Evidence for Sulfur-Based Radicals in Thiolate Compound I Intermediates. *J. Am. Chem. Soc. 121*, 7939−7940.

(19) Licht, S., Gerfen, G. J., and Stubbe, J. A. (1996) Thiyl radicals in ribonucleotide reductases. *Science 271*, 477−481.

(20) Pogni, R., Baratto, M. C., Teutloff, C., Giansanti, S., Ruiz-Dueñas, F. J., Choinowski, T., Piontek, K., Martínez, A. T., Lendzian, F., and Basosi, R. (2006) A Tryptophan Neutral Radical in the Oxidized State of Versatile Peroxidase from *Pleurotus eryngii*: a Combined Multifrequency EPR and Density Functional Theory Study. *J. Biol. Chem. 281*, 9517−9526.

(21) Bernini, C., Pogni, R., Basosi, R., and Sinicropi, A. (2012) The nature of tryptophan radicals involved in the long-range electron transfer of lignin peroxidase and lignin peroxidase-like systems: Insights from quantum mechanical/molecular mechanics simulations. *Proteins: Struct., Funct., Genet. 80*, 1476−1483.

(22) Gray, H. B., and Winkler, J. R. (2015) Hole hopping through tyrosine/tryptophan chains protects proteins from oxidative damage. *Proc. Natl. Acad. Sci. U. S. A. 112*, 10920−10925.

(23) Muller, P., Yamamoto, J., Martin, R., Iwai, S., and Brettel, K. (2015) Discovery and functional analysis of a 4th electron-transferring tryptophan conserved exclusively in animal cryptochromes and (6−4) photolyases. *Chem. Commun. 51*, 15502−15505.

(24) Winkler, J. R., and Gray, H. B. (2015) Electron flow through biological molecules: does hole hopping protect proteins from oxidative damage? *Q. Rev. Biophys. 48*, 411−420.

(25) Kathiresan, M., and English, A. M. (2017) LC-MS/MS suggests that hole hopping in cytochrome c peroxidase protects its heme from oxidative modification by excess H2O2. *Chem. Sci. 8*, 1152−1162.

(26) Ortiz de Montellano, P. R., Ed. (2015) *Cytochrome P450 - Structure, Mechanism, and Biochemistry*, Springer, Switzerland.

(27) Green, M. T., Dawson, J. H., and Gray, H. B. (2004) Oxoiron(IV) in Chloroperoxidase Compound II is Basic: Implications for P450 Chemistry. *Science 304*, 1653−1656.

(28) Behan, R. K., Hoffart, L. M., Stone, K. L., Krebs, C., and Green, M. T. (2006) Evidence for basic ferryls in cytochromes P450. *J. Am. Chem. Soc. 128*, 11471−11474.

(29) Krest, C. M., Onderko, E. L., Yosca, T. H., Calixto, J. C., Karp, R. F., Livada, J., Rittle, J., and Green, M. T. (2013) Reactive Intermediates in Cytochrome P450 Catalysis. *J. Biol. Chem. 288*, 17074−17081.

(30) Rittle, J., and Green, M. T. (2010) Cytochrome P450 Compound I: Capture, Characterization, and C-H Bond Activation Kinetics. *Science 330*, 933−937.

(31) Yosca, T. H., Rittle, J., Krest, C. M., Onderko, E. L., Silakov, A., Calixto, J. C., Behan, R. K., and Green, M. T. (2013) Iron(IV)-hydroxide pK(a) and the Role of Thiolate Ligation in C-H Bond Activation by Cytochrome P450. *Science 342*, 825−829.

(32) Modi, A. R., Dawson, J. H., Hrycay, E. G., and Bandiera, S. M. (2015) Oxidizing Intermediates in P450 Catalysis: A Case for Multiple Oxidants. *Adv. Exp. Med. Biol. 851*, 63−81.

(33) Sutin, N., and Creutz, C. (1978) Properties and Reactivities of the Luminescent Excited States of Polypyridine Complexes of Ruthenium(II) and Osmium(II), in *Inorganic and Organometallic Photochemistry* (Wrighton, M. S., Ed.), pp 1−27, American Chemical Society, Washington, DC.

(34) Creutz, C., Chou, M., Netzel, T. L., Okumura, M., and Sutin, N. (1980) Lifetimes, Spectra, and Quenching of the Excited-States of Polypyridine Complexes of Iron(II), Ruthenium(II), and Osmium(II). *J. Am. Chem. Soc. 102*, 1309−1319.

(35) Ener, M. E., Lee, Y. T., Winkler, J. R., Gray, H. B., and Cheruzel, L. (2010) Photooxidation of cytochrome P450-BM3. *Proc. Natl. Acad. Sci. U. S. A. 107*, 18783−18786.

(36) Girvan, H. M., Seward, H. E., Toogood, H. S., Cheesman, M. R., Leys, D., and Munro, A. W. (2007) Structural and spectroscopic characterization of P450BM3 mutants with unprecedented P450 heme iron ligand sets - New heme ligation states influence conformational equilibria in P450BM3. *J. Biol. Chem. 282*, 564−572.

(37) Park, S.-Y., Yamane, K., Adachi, S.-i., Shiro, Y., Weiss, K. E., Maves, S. A., and Sligar, S. G. (2002) Thermophilic cytochrome P450 (CYP119) from *Sulfolobus solfataricus*: high resolution structure and functional properties. *J. Inorg. Biochem. 91*, 491−501.

(38) Castellano, F. N., Dattelbaum, J. D., and Lakowicz, J. R. (1998) Long-lifetime Ru(II) complexes as labeling reagents for sulfhydryl groups. *Anal. Biochem. 255*, 165−170.

(39) Mines, G. A., Bjerrum, M. J., Hill, M. G., Casimiro, D. R., Chang, I.-J., Winkler, J. R., and Gray, H. B. (1996) Rates of Heme Oxidation and Reduction in Ru(His33)cytochrome *c* at Very High Driving Forces. *J. Am. Chem. Soc. 118*, 1961−1965.

(40) Munro, A. W., Malarkey, K., McKnight, J., Thomson, A. J., Kelly, S. M., Price, N. C., Lindsay, J. G., Coggins, J. R., and Miles, J. S. (1994) The Role of Tryptophan-97 of Cytochrome P450-BM3 from *Bacillus megaterium* in Catalytic Function - Evidence Against the Covalent Switching Hypothesis of P450 Electron Transfer. *Biochem. J. 303*, 423−428.

(41) Coelho, P. S., Wang, Z. J., Ener, M. E., Baril, S. A., Kannan, A., Arnold, F. H., and Brustad, E. M. (2013) A serine-substituted P450 catalyzes highly efficient carbene transfer to olefins in vivo. *Nat. Chem. Biol. 9*, 485−487.

(42) Whited, C. A., Belliston-Bittner, W., Dunn, A. R., Winkler, J. R., and Gray, H. B. (2009) Nanosecond photoreduction of inducible nitric oxide synthase by a Ru-diimine electron tunneling wire bound distant from the active site. *J. Inorg. Biochem. 103*, 906−911.

(43) Dunn, A. R., Dmochowski, I. J., Winkler, J. R., and Gray, H. B. (2003) Nanosecond Photoreduction of Cytochrome P450cam by Channel-Specific Ru-Diimine Electron Tunneling Wires. *J. Am. Chem. Soc. 125*, 12450−12456.

(44) Denisov, I. G., Makris, T. M., and Sugar, S. G. (2002) Cryoradiolysis for the Study of P450 Reaction Intermediates. *Methods Enzymol. 357*, 103−115.